Progress In Electromagnetics Research Letters, Vol. 97, 77–85, 2021

A Novel Miniaturized Bandpass Filter Basing on Stepped-Impedance Resonator

Man Zhang[1], Minquan Li[1, *], Pingjuan Zhang[2], Kaiyue Duan[1], Bao Kun Jin[1], Lichang Huang[1], and Yawen Song[1]

Abstract—This paper proposes a novel miniaturized bandpass filter by loading a stepped-impedance resonator (SIR). Owing to the intrinsic characteristic of SIR, a third-order bandpass filter with SIR is presented, which has a size reduction of 38% compared with the conventional hairpin-line filter. On account of the electrical tape gap effect of a defected ground structure (DGS), further miniaturization is realized by introducing a pair of complementary split-ring resonator (CSRR) DGSs. Besides, frequency selectivity and out-of-band rejection can be improved by adding CSRR DGS and source-load (S-L) coupling structures, which produce two transmission zeros at two side band of passband, respectively. The results show that the passband range is 3.4–3.6 GHz, and the final size is reduced by 50.3%.

1. INTRODUCTION

Miniaturization has been a key issue for microwave components. Filter is an important component of a wireless communication system; thus, techniques for miniaturization have been developed by many researchers. Conventional bandpass filters (BPFs) are usually composed of parallel coupling lines [1, 2], but it leads to a large circuit size. Then, hairpin-line filters come into being [3]. However, they still have the disadvantage of large size. In [4, 5], two kinds of meandered resonators are proposed. Meandered resonators can effectively realize miniaturization compared with conventional half-wavelength resonator. Meander line technique compound with Minkowski fractals introduced in [4] is more complex and requires higher machining accuracy, and insertion loss of the filter proposed in [5] is large. Substrate integrated waveguide (SIW) technology can be a great choice for miniaturization [6, 7]. In [7], an SIW cavity resonator is loaded with stubs on the two side edges, which allows the stub loaded cavity to operate below its resonance frequency, and the dimension is about $1.63\lambda_g \times 0.43\lambda_g$. In 1980, Makimoto et al. [8] first proposed a stepped-impedance resonator (SIR), and SIR has the advantages of small size, easy integration, low cost, and controllable parasitic passband compared with the traditional uniform impedance resonator. Thus, the structure of SIR is widely used in the design of microstrip filters [9–21]. In [9], a filter consists of coupled lines periodically loaded with patch capacitors, and this method provides a slow wave effect to the coupled lines useful for filter miniaturization. Two pairs of embedded E-shaped DGSs are loaded to the half-mode substrate integrated waveguide to realize miniaturization [11]. In [12], a BPF is built up by etching a quad-mode defected ground structure (DGS) resonator, which has two symmetric planes, and the dimension of the proposed filter is $0.76\lambda_g \times 0.69\lambda_g$. In [13], a BPF is made up of a high impedance transmission line as series band-pass filter section and a shunt-connected band-stop section resistively terminated, and the dimension of the proposed filter is $1.15\lambda_g \times 0.58\lambda_g$. In [20], a SIR with an interdigital capacitor structure is proposed to design a BPF, which is manufactured by high-temperature superconducting technology. This kind of filter is compact,

Received 10 February 2021, Accepted 2 April 2021, Scheduled 8 April 2021

* Corresponding author: Minquan Li (AHU411MHz@hotmail.com).

[1] Key Lab of Ministry of Education of Intelligent Computing & Signal Processing, Anhui University, Hefei 230601, China. [2] Anhui Science and Technology University, Bengbu 233100, China.

but it has a high production cost. Above all, the purpose of this paper is to design a filter that meets the design requirements with low production cost, simple structure, high selectivity, and miniaturization.

In this work, a new way for microstrip filter design not only achieves miniaturization but also maintains high selectivity, and deep out-of-band rejection is proposed. The structure proposed in this paper stems from fifth-order hairpin-line filters, which allows for a third-order minimum finally. Firstly, the stepped-impedance resonator structure is configured to a hairpin structure. Additional capacitance is introduced owing to the coupling of the different impedance sections, which shifts down the central frequency of the bandpass filter and enables miniaturization of the filter with the bandwidth and insertion loss intact. Secondly, the size of the structure can be further reduced by adding complementary split-ring resonator (CSRR) DGSs. Therefore, two transmission zeros (TZs) are introduced and located below the passband to enhance selectivity on account of the electrical tape gap effect of DGS. However, the introduction of this method results in poor out-of-band rejection for the upper band of the demand passband. Finally, with the introduction of source-loading (S-L) coupling structure, the required TZs can be obtained and located above the passband to further improve the frequency selectivity and out-of-band rejection. To validate the design scheme, a compact BPF filter centered at 3.5 GHz which is used in IMT-2020 band applications with a fractional bandwidth of 8.86% has been designed based on SIR. The filter has been designed on 0.508 mm-thick Rogers RT/duroid 6002 which has a loss tangent tanδ of 0.0012 and relative dielectric constant ε_r of 2.94. Rogers RT/duroid 6002 microwave material is a low loss and low dielectric constant laminate that offers excellent electrical and mechanical properties when mechanically reliable and electrically stable microwave structures are designed. This plate is modeled and simulated in software HFSS. As a result, a rejection level of more than 53 dB has been obtained along with a size reduction of 50.3%.

2. RESONANT CHARACTERISTICS OF THE SYMMETRIC SIR

Stepped-impedance resonators have the types of 1/4 wave length resonators, half wave length resonators, and full wave length resonators. A configuration of the half wave length symmetric microstrip SIR is shown in Fig. 1(a). The SIR consists of two lines of different characteristics impedances Z_1 and Z_2, of electrical lengths θ_1 and θ_2, and of admittances Y_1 and Y_2. The $ABCD$ matrix of the nonuniform structure can be obtained as:

$$\begin{bmatrix} A & B \\ C & D \end{bmatrix} = \begin{bmatrix} \cos\theta_2 & jZ_1\sin\theta_2 \\ j\dfrac{\sin\theta_2}{Z_2} & \cos\theta_2 \end{bmatrix} \begin{bmatrix} \cos 2\theta_1 & jZ_2\sin 2\theta_1 \\ j\dfrac{\sin 2\theta_1}{Z_1} & \cos 2\theta_1 \end{bmatrix} \begin{bmatrix} \cos\theta_2 & jZ_1\sin\theta_2 \\ j\dfrac{\sin\theta_2}{Z_2} & \cos\theta_2 \end{bmatrix} \tag{1}$$

The input admittance Y_{in} of the symmetric SIR can be given as:

$$Y_{in} = jY_2 \frac{2(K\tan\theta_1 + \tan\theta_2)\cdot(K - \tan\theta_1\cdot\tan\theta_2)}{K(1-\tan^2\theta_1)(1-\tan^2\theta_2) - 2(1+K^2)\cdot\tan\theta_1\cdot\tan\theta_2} \tag{2}$$

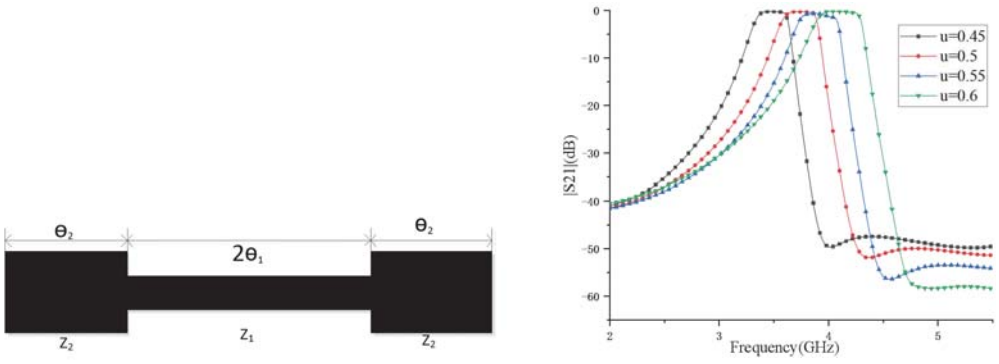

(a) (b)

Figure 1. (a) Basic structure of the half wave length SIR. (b) Sweeping the parameter u.

where K is the characteristic impedance ratio Z_2/Z_1, and the resonance condition can be obtained when Y_{in} is equal to zero. Thus, the fundamental resonance frequency can be expressed as:

$$K = \tan\theta 1 \cdot \tan\theta 2 \tag{3}$$

Taking the spurious resonance frequency to be f_{sn} $(n = 1, 2, 3...)$, the first spurious resonance occurs at:

$$\tan\theta_{s1} = \infty \tag{4}$$

where θ_{s1} is the electrical length for the first spurious frequency at f_{s1}. From Eqs. (3) and (4), we obtain:

$$\frac{f_{s1}}{f_0} = \frac{\theta_{s1}}{\theta_0} = \frac{\pi}{2\tan^{-1}\sqrt{K}} \tag{5}$$

It becomes clear from Eq. (5) that the spurious response can be controlled by the impedance ratio K. In Fig. 1(b), it is shown that the center frequency of the passband moves down with the decrease of u, where u is the electrical length ratio θ_2/θ_1. Accordingly, the SIR should be implemented to realize miniaturization as discussed in the next section.

3. DESIGN AND ANALYSIS

3.1. Design of Third-Order Filter

The proposed Chebyshev-type bandpass filter has the specifications of center frequency $f_0 = 3.5\,\text{GHz}$, fractional bandwidth FBW = 8.86%, and passband ripple $L_{\text{Ar}} = 0.5\,\text{dB}$. The order of the filter has been calculated as five, and the layout of the conventional filter is shown in Fig. 2. The order of the conventional filter can be reduced to three with the introduction of SIR on account of the special coupling scheme between Z_1 and Z_2 sections. The input and output sections are modified by folding it by 90°

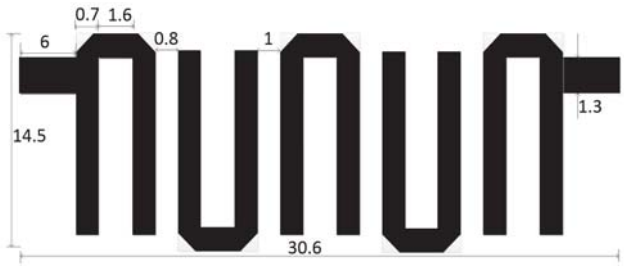

Figure 2. Layout of conventional fifth-order BPF.

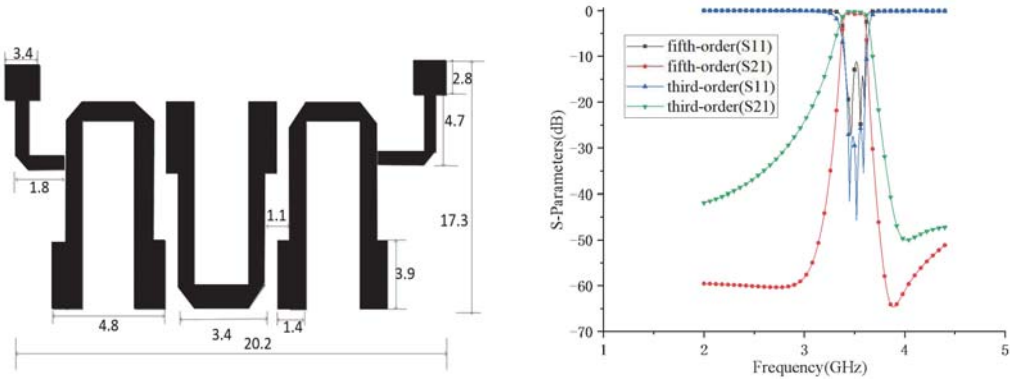

(a) (b)

Figure 3. (a) Layout of third-order BPF. (b) Comparison of S-parameters between the conventional and third-order filters.

to miniaturize the effective area. Tapering with 45° of the bent edges has been performed to reduce the radiation effects for the abrupt change of surface current flow. Thus, the layout of the improved filter is more compact as shown in Fig. 3(a). Fig. 3(b) compares the simulated S_{11} and S_{21} between the conventional and third-order filters. It has been observed that the required central frequency, relative bandwidth, insertion loss, and return loss are satisfied. However, the stopband rejection on both sides of the passband is reduced. Hence, in Section 3.2, we shall pay attention to the enhancement of stopband rejection for the passband filter, especially on the upper stopband.

3.2. Analysis of CSRR DGS

The layout of a CSRR is presented in Fig. 4(a), which is etched on the metallic ground plane. This kind of DGS distracts the current distributions, resulting in the alterations of the transmission line property [14]. CSRR DGS can be equivalent to a resonant LC tank as shown in Fig. 4(b). The equivalent circuit can be achieved by structure analysis, current flow analysis, and S-parameters curve fitting. The current flow around the edges of DGS can be equivalent by capacitance and inductance.

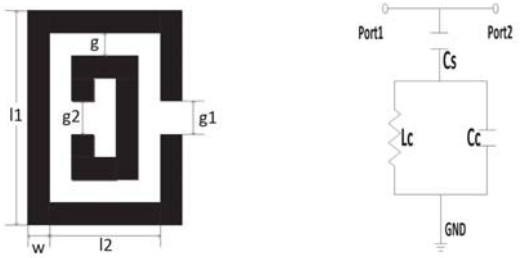

Figure 4. (a) Topology. (b) The equivalent circuit model of the square CSRR.

The detailed parameters of the equivalent circuit can be driven as:

$$C_s = \frac{f_c^2 \,/\, f_0^2 - 1}{\pi f_c Z_0 (f_c^2 \,/\, f_n^2 - 1)} \tag{6}$$

$$L_c = \frac{1}{4\pi^2 C_s} \left(\frac{1}{f_0^2} - \frac{1}{f_n^2} \right) \tag{7}$$

$$C_c = \frac{1}{(2\pi f_n)^2 L_c} \tag{8}$$

where f_n is the zero point of the reflection coefficient (S_{11}), f_0 the zero point of the reflection coefficient (S_{21}), and f_c the 3 dB cutoff frequency. The matrix can be expressed as:

$$M = \begin{bmatrix} 1 & 0 \\ Y_{Cg} & 1 \end{bmatrix} \tag{9}$$

where $Y_{Cg} = jwC_s(1 - w^2 L_c C_c)/[1 - w^2 L_c(C_c + C_s)]$.

The resonance frequencies (f_s) of the CSRR DGS with different lengths (l_1) and widths (w) are illustrated in Figs. 5(a) and (b). With the increase of $l1$, the additional inductance becomes larger, then the resonant frequency moves to lower frequency. And the resonant frequency moves to the upper frequency with the increase of w, which causes the decrease of the additional capacitance. Therefore, geometry parameters of the DGS can be adjusted which produces a shift in the central frequency to achieve the purpose of miniaturization.

According to the mentioned analysis, the CSRR oriented face-to-face can be applied to the bandpass filter designed in the Section 3.1. The layout of the third-order BPF with DGS is shown in Fig. 6(a). The coupling between the adjacent hairpin-line units can be enhanced obviously, which produces a shift to lower area in the central frequency. Therefore, further miniaturization is achieved with the comparison

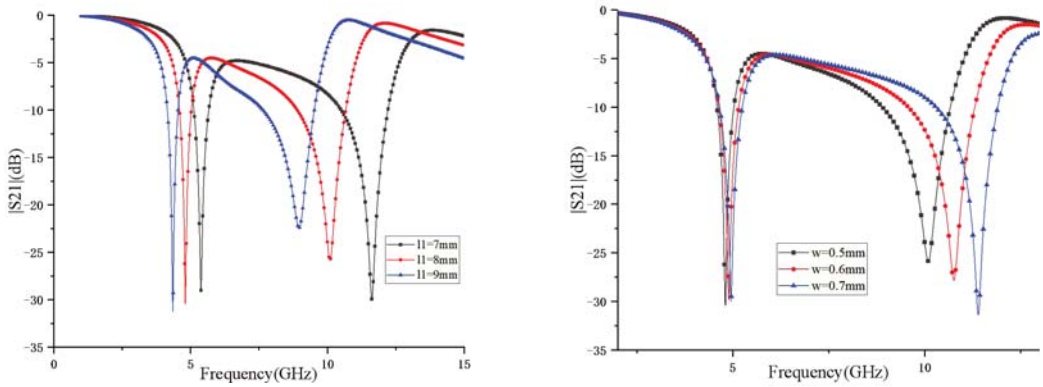

Figure 5. The resonant characteristic of CSRR DGS.

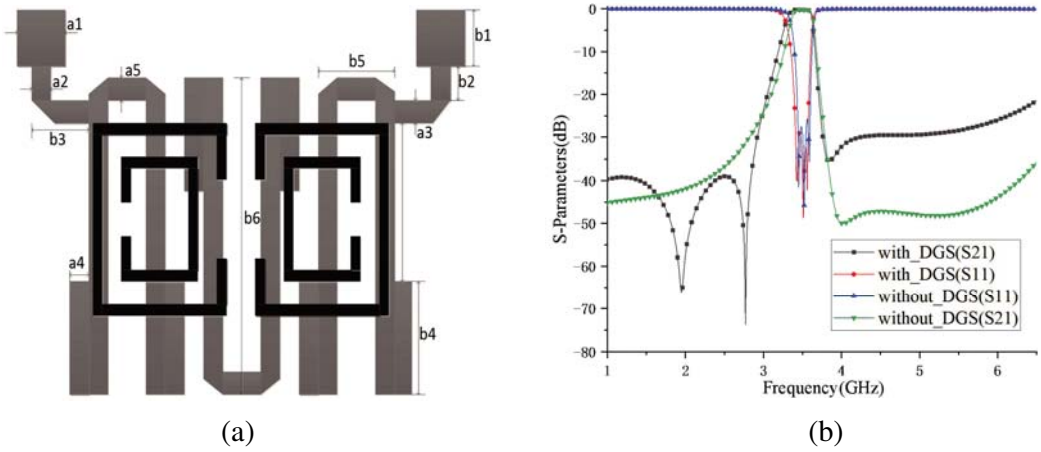

Figure 6. (a) Layout of third-order filter with DGS. (b) Comparison of S-parameters.

of the design in previous section. Besides, the addition of the CSRR DGS can introduce two TZs on the lower stopband to realize selectivity and lower stopband rejection improvement. However, it can be observed from Fig. 6(b) that the upper stopband rejection becomes poorer than before. The solution of this drawback will be discussed in the next section.

3.3. Optimization Based on S-L Coupling

Source-load coupling brings multiple TZs [22]. Fig. 7(a) displays the layout of the improved filter with an I/O port that consists of a feeding line and a parallel coupling arm. The parallel coupling arm is called source-load coupling, and the coupling topology scheme is illustrated in Fig. 7(b). There are two coupling paths for the signal from the source to load. One path is tagged according to the order, resonator 1-2-3, and the other is directly from the source to load which is denoted by the dashed line in Fig. 7(b). As a result, one TZ can be obtained on the upper stopband, then the out-of-band rejection of the filter is improved obviously. The length (w_1) and gap width (s) can be sightly adjusted to reach coupling strength enhancement. Hence, the TZ in the stopband will split from one to two as shown in Figs. 8(a) and (b), resulting in greater out-of-band rejection. Compared with the filter designed in Section 3.2, the filter with a source-load coupling has higher out-of-band rejection which is shown in Fig. 8(c). The final circuit sizes are as follows (unit: mm): $a_1 = 3.6$, $a_2 = 0.7$, $a_3 = 1$, $a_4 = 0.8$, $a_5 = 0.5$, $b_1 = 2.6$, $b_2 = 3.2$, $b_3 = 3$, $b_4 = 4.1$, $b_5 = 2$,$b_6 = 11.4$, $l_1 = 7.7$, $l_2 = 3$, $g = 0.5$, $g_1 = 4.7$, $g_2 = 1.5$, $w = 0.2$, $w_1 = 0.5$, $s = 0.6$.

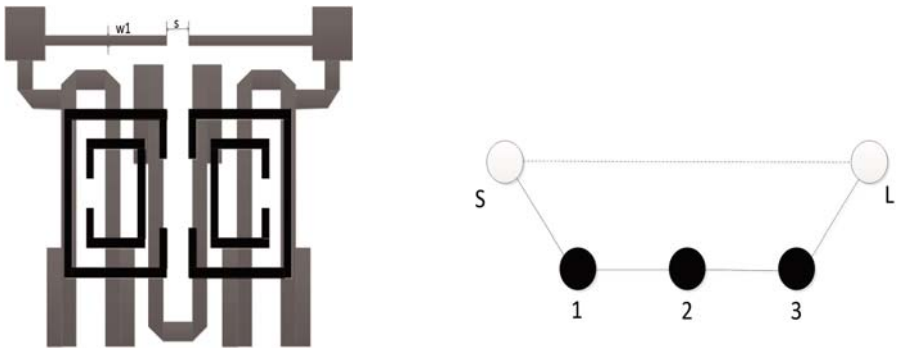

(a) (b)

Figure 7. (a) Layout of the proposed filter. (b) Coupling scheme for the proposed filter.

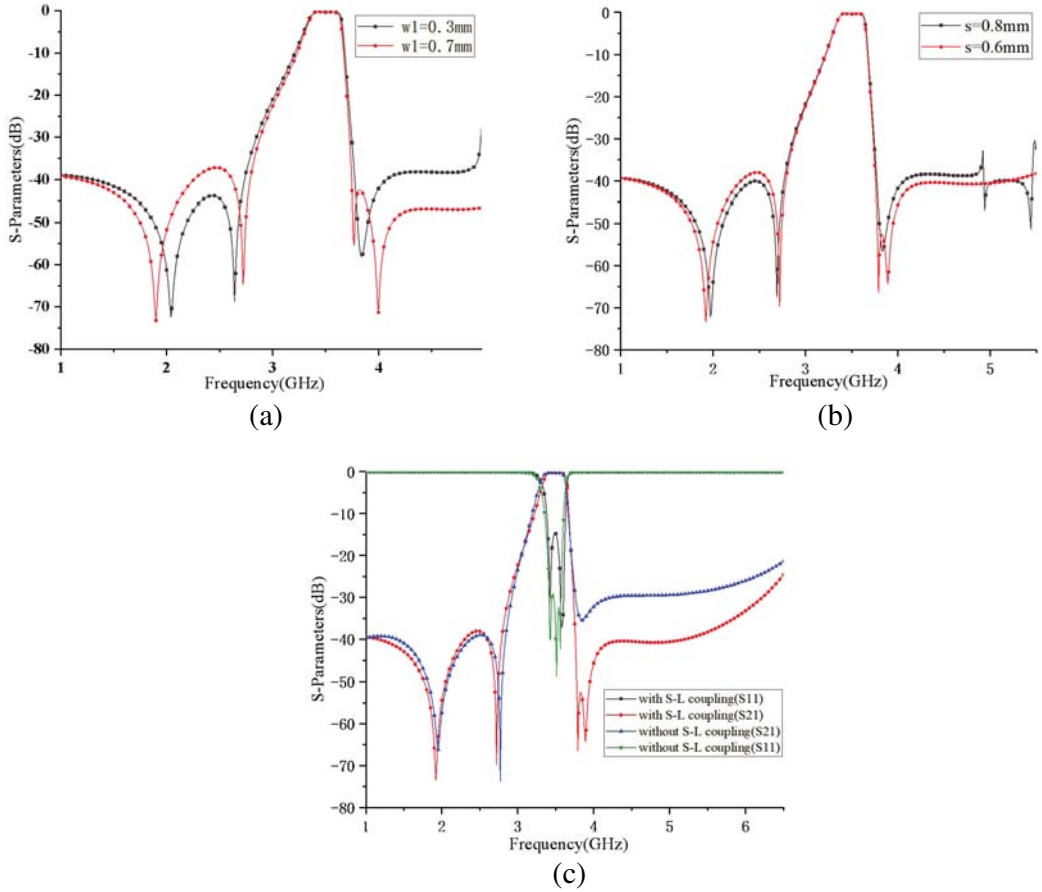

(a) (b)

(c)

Figure 8. (a) Response changed with the length (w_1). (b) Response changed with the gap width (s). (c) Filter with and without S-L coupling.

4. MEASUREMENT AND ANALYSIS

To validate the proposed design flow, four filters are simulated, fabricated, and measured. The simulation is taken using EM-simulator HFSS. Using this EM-simulator, we simulate the current distributions in the proposed BPF at (a) 2.5 GHz, (b) 3.0 GHz, (c) 3.5 GHz, and (d) 4.0 GHz, shown in Fig. 9. As a result, at the resonance condition, the reactive components are canceled by each other and

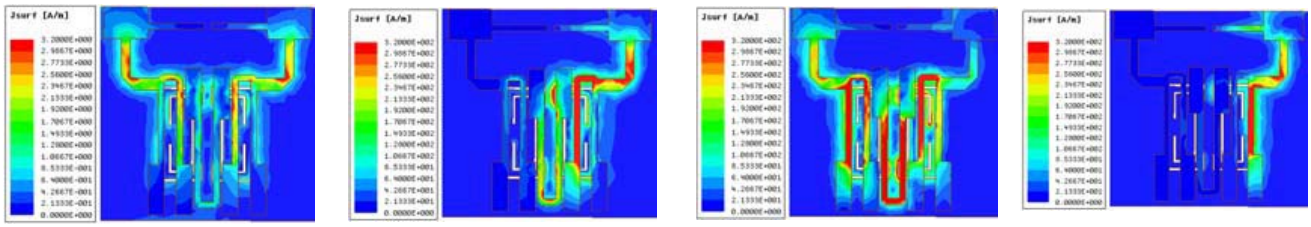

Figure 9. The current distributions in the proposed filter at (a) 2.5 GHz, (b) 3.0 GHz, (c) 3.5 GHz, and (d) 4.0 GHz frequencies.

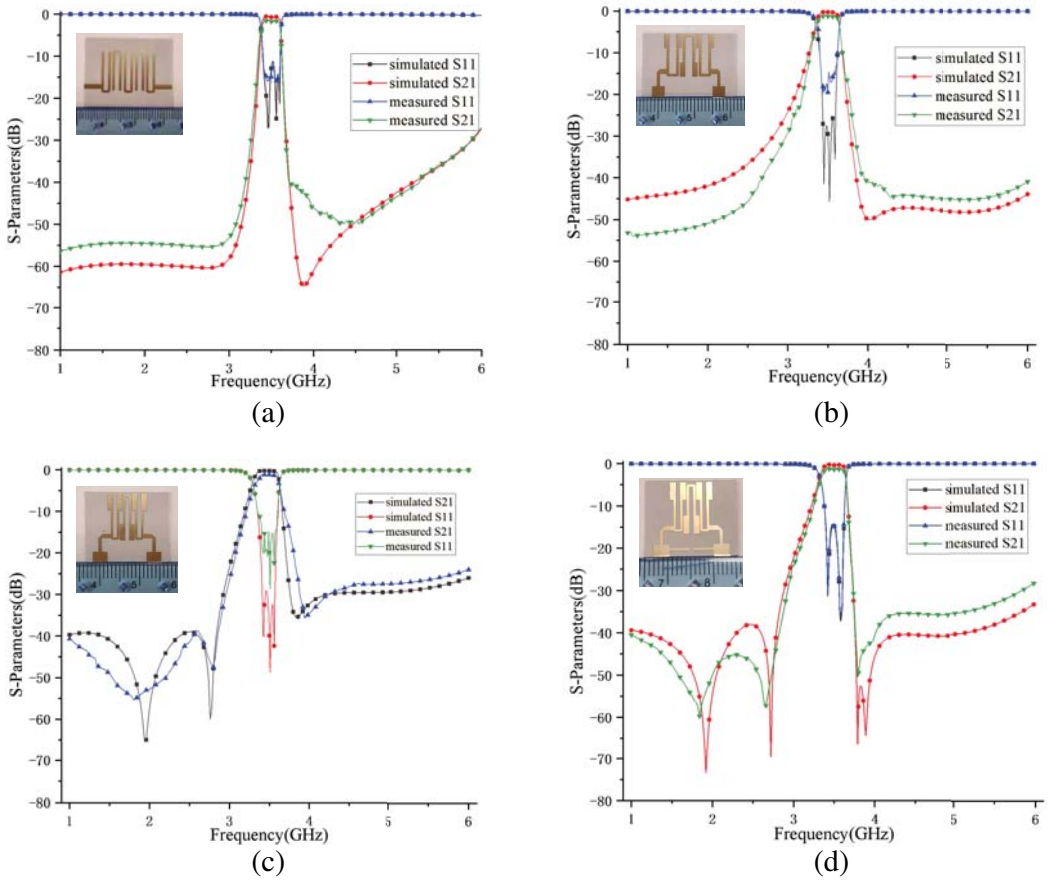

Figure 10. Simulated, measured results and photos of the designed filters.

leave only the resistance, resulting in the maximum current flowing in that condition rather than those found in the other nonresonance frequency bands.

Compared with the results in Figs. 10(a) and (b), a size reduction has been realized from $30.6 \times 23.8\,\text{mm}^2$ to $25.8 \times 17.5\,\text{mm}^2$ by introducing SIR. Compared with the results in Figs. 10(b) and (c), two TZs are introduced and located below the passband by CSRR DGS. It realizes a further size reduction from $25.8 \times 17.5\,\text{mm}^2$ to $20.8 \times 17.6\,\text{mm}^2$ at the sacrifice of upper out-of-band rejection. Compared with the results in Figs. 10(c) and (d), with the adoption of source-load coupling, two TZs are introduced and located above the passband to achieve higher out-of-band rejection but with other performance intact. Due to mismatching tolerance and parasitic effect of soldering, the TZs shown above the passband are reduced from two to one compared with the simulated result. It can be seen from Fig. 10(d) that the passband range is 3.4–3.6 GHz, and the frequency selectivity is also great. Besides,

Table 1. Comparison of various BPF.

Reference	f_0 (GHz)	IL (dB)	TZs	Roll off rate/GHz Lower, Upper	Size ($\lambda_g \times \lambda_g$)
[2]	4	3.23	2	80/92.81	2.36×0.75
[6]	5.2	2.2	0	36/30	2.23×1.28
[7]	5.8	2.25	2	60/54	1.63×0.43
[12]	2.45	1.98	3	45 /302	0.76×0.69
[13]	1.97	0.71	2	50/46	$1.15\times$ 0.58
[15]	2	1.7	2	235/184	1.04×0.29
[16]	2.4	2	2	218/168	0.76×0.38
[17]	5.85	1.6	2	64.3/76	0.57×0.57
[18]	1.8	2.5	2	400/370	1.48×0.74
This Work	3.5	1.6	4	109.26/422.27	0.4×0.35

the final size of this BPF is $20.8 \times 17.4\,\mathrm{mm}^2$ which achieves 50.3% size minimization in comparison with the conventional fifth-order BPF. The measurement results verify the feasibility of the BPF design method. Compared with the previous works, the BPF designed in this paper has excellent frequency selectivity with compact size. There is a systematic comparison in Table 1.

5. CONCLUSION

A novel bandpass filter using SIR is proposed. The order of BPF has been decreased by introducing SIR which realizes miniaturization. DGS and source-load coupling structure introduce multiple TZs to improve frequency selectivity. As a result, the proposed filter achieves 50.3% size minimization with the performance of the bandpass filter intact. The simulated and measured results have a good agreement, which show that the proposed filter features compact size, sharp skirt, and proves that the proposed structure has a more extensive application than the conventional one.

ACKNOWLEDGMENT

This work is supported by the Key Natural Science Research Project of Anhui Higher Education Institutions: Research on Environmental RF Energy Harvesting System KJ2019A0804, and the National Nature Science Foundation of China 51477001.

REFERENCES

1. Tsai, C. and H. Lee, "Improved design equations of the tapped-line structure for coupled-line filters," *IEEE Microwave and Wireless Components Letters*, Vol. 17, No. 4, 244–246, April 2007.
2. Marín, S., J. D. Martínez, and V. E. Boria, "Realization of filters with improved selectivity using lumped and quasi-lumped terminating half sections," *2017 47th European Microwave Conference (EuMC)*, 636–639, Nuremberg, 2017, doi: 10.23919/EuMC.2017.
3. Sánchez-Renedo, M., R. Gómez-Garcia, and R. Loeches-Sánchez, "Microstrip filters with selectivity improvement using the new concept of signal-interference source/load coupling," *2013 IEEE MTT-S International Microwave Symposium Digest (MTT)*, 1–4, Seattle, WA, 2013, doi: 10.1109/MWSYM.2013.6697325.
4. Marzah, A. A. and J. S. Aziz, "Design and analysis of high performance and miniaturized bandpass filter using meander line and, Minkowski fractal geometry," *2018 Al-Mansour International Conference on New Trends in Computing, Communication, and Information Technology (NTCCIT)*, 12–17, Baghdad, Iraq, 2018, doi: 10.1109/NTCCIT.2018.8681174.

5. Ma, K., K. S. Yeo, J. Ma, and M. A. Do, "An ultra-compact hairpin band pass filter with additional zero points," *IEEE Microwave and Wireless Components Letters*, Vol. 17, No. 4, 262–264, April 2007.
6. Riaz, L., U. Naeem, and M. F. Shafique, "Miniaturization of SIW cavity filters through stub loading," *IEEE Microwave and Wireless Components Letters*, Vol. 26, No. 12, 981–983, December 2016.
7. Pu, J., F. Xu, and Y. Li, "Miniaturized substrate integrated waveguide bandpass filters based on novel complementary split ring resonators," *2019 IEEE MTT-S International Microwave Biomedical Conference (IMBioC)*, 1–3, Nanjing, China, 2019.
8. Makimoto, M., K. Kikuchi, and S. Yamashita, "Compact TV channel filters in the UHF band," *IEEE Transactions on Cable Television*, Vol. CATV-5, Issue 4, 164–168, 1980.
9. Orellana, M., et al., "Design of capacitively loaded coupled-line bandpass filters with compact size and spurious suppression," *IEEE Transactions on Microwave Theory and Techniques*, Vol. 65, No. 4, 1235–1248, April 2017.
10. Lee, S. and Y. Lee, "Generalized miniaturization method for coupled-line bandpass filters by reactive loading," *IEEE Transactions on Microwave Theory and Techniques*, Vol. 58, No. 9, 2383–2391, September 2010.
11. Wang, C., Z. Wang, and Y. M. Huang, "Size-miniaturized half-mode substrate integrated waveguide bandpass filter incorporating E-shaped defected ground structure for wideband communication and radar applications," *2018 20th International Conference on Advanced Communication Technology (ICACT)*, 12–16, Chuncheon, Korea (South), 2018, doi: 10.23919/ICACT.2018.8323628.
12. Peng, B., et al., "Compact quad-mode bandpass filter based on quad-mode DGS resonator," *IEEE Microwave and Wireless Components Letters*, Vol. 26, No. 4, 234–236, April 2016.
13. Luo, C., et al., "Quasi-reflectionless microstrip bandpass filters using bandstop filter for out-of-band improvement," *IEEE Transactions on Circuits and Systems II: Express Briefs*, Vol. 67, No. 10, 1849–1853, October 2020.
14. Liu, H., et al., "High-temperature superconducting bandpass filter using asymmetric stepped-impedance resonators with wide-stopband performance," *IEEE Transactions on Applied Superconductivity*, Vol. 25, No. 5, 1–6, Oct. 2015.
15. Chen, C., "A coupled-line coupling structure for the design of quasi-elliptic bandpass filters," *IEEE Transactions on Microwave Theory and Techniques*, Vol. 66, No. 4, 1921–1925, April 2018.
16. Tang, C. and M. Chen, "Wide stopband parallel-coupled stacked SIRs bandpass filters with open-stub lines," *IEEE Microwave and Wireless Components Letters*, Vol. 16, No. 12, 666–668, December 2006.
17. Maharjan, R. K., et al., "Miniature stubs-loaded square open-loop bandpass fliter with asymmetrical feeders," *Microwave and Optical Technology Letters*, Vol. 55, No. 2, 329–332, February 2013.
18. Sheikhi, A., A. Alipour, and A. Mir, "Design and fabrication of an ultra-wide stopband compact bandpass filter," *IEEE Transactions on Circuits and Systems II: Express Briefs*, Vol. 67, No. 2, 265–269, February 2020.
19. Das, et al., "2nd harmonic suppression in parallel-coupled microstrip bandpass filter by using Koch fractals," *2016 IEEE Annual India Conference (INDICON)*, 1–6, Bangalore, India, 2016.
20. Luo, C., et al., "A wide stopband wideband HTS filter using stepped-impedance resonators with an interdigital capacitor structure," *IEEE Transactions on Applied Superconductivity*, Vol. 30, No. 2, 1–5, March 2020.
21. Han, C., Y. Rao, H. J. Qian, and X. Luo, "High-selectivity bandpass filter with wide upper stopband using harmonic suppression structure," *2019 IEEE International Symposium on Radio-Frequency Integration Technology (RFIT)*, 1–3, Nanjing, China, 2019.
22. Ieu, W., D. Zhou, D. Zhang, et al., "Compact dual-mode dual-band HMSIW bandpass filters using source-load coupling with multiple transmission zeros," *Electronics Letters*, Vol. 55, No. 4, 210–222, 2019.